




# Synergetic impact of natural light harvesting materials to reduce the recombination rate and improve the device performance of dye sensitized solar cells

Amutha Soosairaj<sup>1</sup>, Durga Prasad Pabba<sup>2</sup>, Ahalya Gunasekaran<sup>3</sup>, Sambandam Anandan<sup>3</sup>, Joseph Selvaraj<sup>4</sup>, and Leo Rajesh Asirvatham<sup>1,\*</sup> 

<sup>1</sup> Department of Physics, St. Joseph's College (Autonomous), Affiliated to Bharathidasan University, Tiruchirappalli 620002, India

<sup>2</sup> Departamento de Mecanica, Facultad de Ingenieria, Universidad Technologica Metropolitana, Santiago, Chile

<sup>3</sup> Nanomaterials and Solar Energy Conversion Lab, Department of Chemistry, National Institute of Technology, Tiruchirappalli 620 015, India

<sup>4</sup> Department of Chemistry, St. Joseph's College (Autonomous), Affiliated to Bharathidasan University, Tiruchirappalli 620002, India

**Received:** 6 May 2023

**Accepted:** 16 August 2023

**Published online:**

2 September 2023

© The Author(s), under exclusive licence to Springer Science+Business Media, LLC, part of Springer Nature, 2023

## ABSTRACT

Natural pigments extracted from *Arachis hypogaea* flowers and *Cassia grandis* leaves were used as novel light harvesting materials for the first time in the fabrication of dye-sensitized solar cells (DSSCs). The extracted individual dyes were labelled as AH, CG and the mixture as AC. The absorption spectra confirmed xanthophyll and chlorophyll pigments in AH, CG and AC with the bandgap of 2.64 eV, 2.7 eV, 2.62 eV. Fourier transform infrared spectroscopy (FTIR) was employed to identify the functional groups present in the dyes. The microstructure, homogeneity, porosity, compositional analysis and roughness of bare and dye loaded TiO<sub>2</sub> films were examined using field emission scanning electron microscopy (FESEM), Energy Dispersive X-ray spectroscopy (EDAX) and Atomic force microscopy (AFM). The photovoltaic performance was evaluated through Current–voltage characteristics (J–V), Electrochemical impedance spectroscopy analysis (EIS) and Bode phase plot analysis. The findings revealed that DSSC with co-sensitized dye (AC) exhibited  $V_{oc}$  of 533 mV,  $J_{sc}$  of 0.42 mA cm<sup>-2</sup> and FF of 0.29 with an improved efficiency that was 1.4 and 2.11 times greater than AH and CG dye based devices respectively. The results proved co-sensitization to be an effective approach to increasing the spectral range and device performance of dye sensitized solar cells.

Address correspondence to E-mail: aleorajesh@gmail.com

## 1 Introduction

The sun, which is regarded as the most fundamental renewable energy source available today, provides energy to each and every organism on earth. The primary advantage of solar energy is that it could be easily harnessed in residential as well as commercial environments. Since solar energy possesses the ability to be transformed into useful heat or power, researchers and engineers are working to develop solar-powered systems that directly use solar energy to produce power [1]. The development of solar cells has advanced, making it possible to make solar cells that are more affordable, lighter, biocompatible and environmentally benign [2]. Dye-sensitized solar cells that imitate photosynthesis in plants were initially developed by Gratzel and O' Regan and have been the subject of substantial research in recent years owing to their affordability and resource-unlimited qualities [3]. It is a third-generation photovoltaic technology that uses synthetic or natural dyes as light-harvesting pigments as opposed to the more well-known silicon devices [4]. The photovoltaic performance of DSSCs is highly dependent on the molecular structure of the dye sensitizers that absorb sunlight and produce excitons [5].

Various types of photosensitizers, including organic dyes, ruthenium and platinum complexes have been employed in DSSC till today. Some of these compounds, however, exhibit severe toxicity and are extremely rare in nature, indicating a difficult, pricey, and non-ecological process of fabrication [6]. Natural dyes thus serve as an affordable replacement for synthetic inorganic and organic dyes due to their

availability, affordability, ease of manufacture, complete biodegradability and environmental friendliness [7]. In nature, some kinds of flowers, fruits, leaves, roots and stems display various hues and contain small amounts of pigment that are efficiently extractable and used as sensitizers in DSSCs [8]. Natural dyes contain carbonyl, carboxylic and hydroxyl groups, which chelate with TiO<sub>2</sub> and enable efficient charge transfer from dye molecules to the conduction band of TiO<sub>2</sub>. Yet, DSSC with natural dyes has a poor track record for stability and efficiency [4]. Therefore, each research step that improves the energy conversion efficiency or cell performance with sensitizers would be beneficial.

PA Ahmad et.al. fabricated natural DSSCs with carissa spinuram, iresine herbstii and ipomoea purpurea dyes and found the highest photovoltaic response of 1.19% for Carissa spinuram based DSSC [7]. GFC Mejica et.al. obtained the best light-to-electricity conversion efficiency of 0.1021% with Malabar spinach fruits at pH 9 [9]. Many natural dyes had been combined together to increase the performance of DSSCs. The previously reported photovoltaic parameters of the co-sensitized natural dyes used in the fabrication of DSSCs are listed in Table 1.

Several natural pigments including carotenoid, chlorophyll, betalain and anthocyanin have been used as sensitizers in DSSCs [9]. Xanthophylls are one of the significant parts of carotenoids and are responsible for the yellow colour in plants. The two main kinds of carotenoids are xanthophylls and carotenes, both of which have a backbone that is either straight or contains cyclic end groups as shown in Fig. 1a [21]. Chlorophylls are metal complexes with

**Table 1** Photovoltaic parameters of co-sensitized natural dyes in DSSCs

Co—sensitized natural dyes	$J_{sc}$ (mA cm <sup>-2</sup> )	$V_{oc}$ (V)	FF	%	Ref
Cactus, Bermuda	3.39	0.464	0.38	0.606	[10]
Cladode, Aloe vera	0.290	0.440	0.40	0.5	[11]
H. sabdariffa, B vulgaris	0.883	0.23	0.69	3.73	[12]
M. verticillate, S. cumini	3.15	0.39	0.37	1.84	[13]
Black rice, P amaryllifolius	2.64	0.46	0.63	0.81	[14]
T. occidentalis, C. pulcherrima	2.91	0.64	0.61	1.14	[15]
B. alba, A. dubius	4.273	0.385	0.51	0.847	[16]
Ixora sp, C. odontophyllum	6.26	0.384	0.47	1.13	[17]
Chinar, Chrysanthemum	0.21	0.502	0.11	3.19	[18]
A. bisporus, C. limonum	1.91	0.489	0.57	0.54	[19]
L. frutescens, E. microphylla	2.55	0.516	0.85	1.33	[20]
A. hypogaea C. grandis	0.42	533	0.29	0.76	Present Work

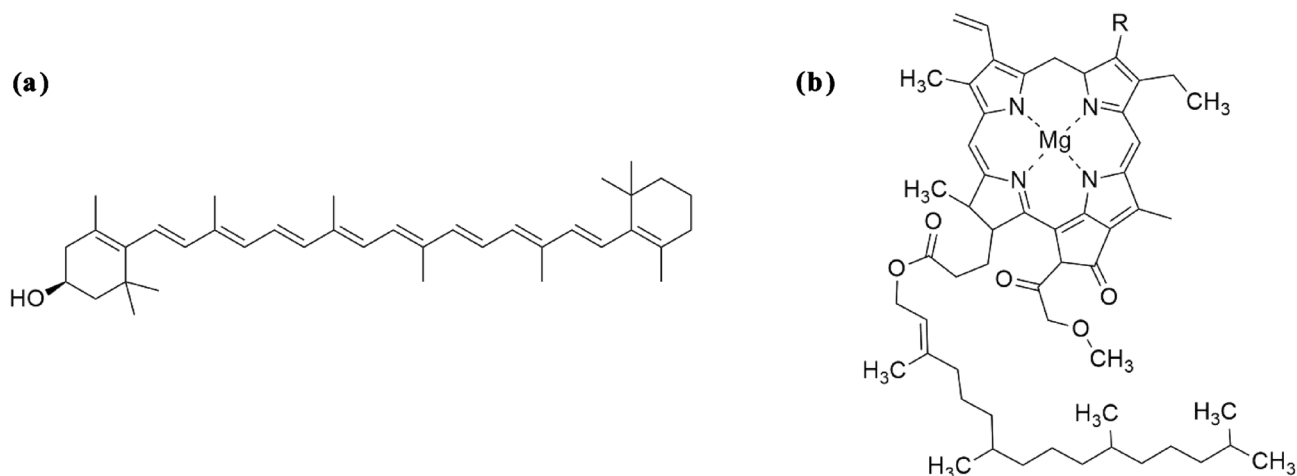


**Fig. 1** Molecular structure of (a) Xanthophyll (b) Chlorophyll natural pigments

great symmetry that contain a core magnesium ion linked to a tetrapyrrolic macrocycle (Fig. 1b) that enable photosynthesis in green plants. The primary function of chlorophylls is collecting light energy, exhibiting spectral properties and transferring energy for photosynthesis [22].

The objective of the present work is to fabricate DSSCs with two natural dyes and their combination and study their optical, functional, morphological, photovoltaic parameters. Two new natural plant-based dyes were derived from *Arachis hypogaea* flowers and *Cassia grandis* leaves and employed as sensitizers in DSSCs in which the highest efficiency of 0.76% was achieved by co sensitization technique. When chlorophyll and xanthophyll dyes were combined, an increase in  $P_{max}$ ,  $V_{oc}$ , FF and conversion efficiency ( $\eta$ ) was seen compared to when both dyes were used individually. To the best of our knowledge, this is the first time that natural dyes derived from these plants have been reported to fabricate DSSCs through co-sensitization.

## 2 Experimental section

### 2.1 Materials

TiO<sub>2</sub> powder (anatase, particle size ~ 25 nm), Triton X-100, Fluorine-doped tin oxide (FTO) conducting glass (resistivity 7Ω/sq., transmittance > 80%), polyethylene glycol (PEG, M.W 10,000), Ethanol,

Potassium iodide (KI), Iodine (I<sub>2</sub>) Hydrochloric acid (HCL), Citric acid (C<sub>6</sub>H<sub>8</sub>O<sub>7</sub>), Titanium (IV) isopropoxide and H<sub>2</sub>[Pt(Cl)<sub>6</sub>] were purchased from Sigma Aldrich.

### 2.2 TiO<sub>2</sub> paste and photoanode preparation

1 gm of TiO<sub>2</sub> nanopowder (Degussa P25), 1 ml of citric acid (0.1 M), 0.2 ml of titanium (IV) isopropoxide, 0.05 ml of non-ionic surfactant triton X-100, and 0.1 ml of polyethylene glycol were taken in a beaker to create TiO<sub>2</sub> paste. The materials were then mixed with a glass rod thoroughly for a few minutes and sonicated for about 20 min to obtain a homogeneous paste [23]. To prepare photoanode, the scotch tape strips were attached to the edges of the FTO with the conducting side facing up, to limit the thickness and control the active region of the TiO<sub>2</sub> film for dye adsorption. The doctor blade technique was used to apply the obtained TiO<sub>2</sub> paste on FTO glass plates with an active area of 0.25 cm<sup>2</sup> to create a homogenous layer of TiO<sub>2</sub> thin film, and the process was repeated till the homogeneity of the film was achieved. The films were then calcined at 450 °C for 2 h on a hot plate to improve the firmness and crystallinity of the films.

### 2.3 Preparation of counter electrode and Electrolyte

Using the spin coating method, platinum solution (4 mM) of H<sub>2</sub>[Pt(Cl)<sub>6</sub>] was coated in a clean FTO plate to produce platinum counter electrodes, which were

then annealed at 450 °C for 30 min.  $I^-/I_3^-$  redox couple was used as liquid electrolyte in the fabrication of DSSCs. The electrolyte solution was prepared by dissolving 0.83 g of potassium iodide (KI) and 0.127 g of iodine ( $I_2$ ) in 10 ml of ethylene glycol [24]. The prepared electrolyte was stored in a black bottle and kept away from atmospheric air and light source.

## 2.4 Preparation of sensitizers

*Arachis hypogaea* flowers and *Cassia grandis* leaves were collected from the fields in Tanjore District in the southern part of Tamilnadu. *Arachis hypogaea* flowers is commonly known as Groundnut flowers and *Cassia grandis* is known as Konrai. The collected plant materials were washed thoroughly with distilled water, air dried for an hour and crushed in to small pieces for further extraction. Using the analytical balance, 30 g of *A. hypogaea* and *C. grandis* were immersed in 50 ml of ethanol in separate beakers. The beakers were then closed with aluminum foil and kept away from light for 24 h. The extracts were then filtered with whatmann filter paper [6, 19] and the resultant dye solutions were employed as individual and combined sensitizers for the fabrication of DSSCs and further characterization. The individual dye extracts of *Arachis hypogaea* was designated as AH and *Cassia grandis* as CG. The combination of these both dyes with 1:1 volume ratio was named as AC.

## 2.5 Fabrication of DSSC

The as prepared pure  $TiO_2$  films were immersed in AH, CG and AC dye solutions at room temperature for 24 h in dark. The dye stained  $TiO_2$  films were then removed from the extracts and washed with ethanol to remove the debris from the electrodes. Using the Stylus profilometer, the thicknesses of the pure  $TiO_2$  film and dye stained  $TiO_2$  films were found to be  $\sim 9.8 \mu m$  and  $\sim 10.1 \mu m$  respectively. To assemble the DSSCs, the dye anchored  $TiO_2$  photoanode and platinum counter electrode were clipped with binder clips facing each other. A few drops of electrolyte solution were applied between the electrodes using capillary action. The ethanolic extracted natural sensitizers, dye anchored films, fabricated devices and the corresponding current–voltage output are diagrammatically represented in Fig. 2.

## 2.6 Characterization and measurements

The absorption spectra of single, mixture dyes and sensitized films were recorded using UV–visible spectrophotometer (Perkin Elmer Lambda 35). The FTIR spectra for dye extracts were analysed through FT-IR spectroscopy (Perkin Elmer spectrum RX-1). Stylus profilometer (Mitutoyo SurfTest SJ-401) was used to find the thickness of  $TiO_2$  films. The surface morphology of pure  $TiO_2$  and the sensitized films was done using (FESEM) Field emission scanning electron microscopy and the compositional analysis of pure  $TiO_2$  thin film was analysed through Energy Dispersive X-ray spectroscopy (Gemini ZEISS–1). The surface roughness of the pure  $TiO_2$  film was examined by Atomic force microscopy (AFM, Model BT02218, Nanosurf). The solar energy conversion efficiency of the fabricated DSSCs was measured using a computerized solar simulator (AM 1.5,  $85 mWcm^{-2}$ ) with an Oriel 150 W Xe light source. The open circuit voltage ( $V_{oc}$ ), short circuit current density ( $J_{sc}$ ), fill factor (FF) and the photo-conversion efficiency ( $\eta$ ) of the devices were determined through J-V curve. For measuring the electrochemical properties of the cells, AUTOLAB12/FRA2 electrochemical analyzer was used. The incident photon to current conversion efficiency (IPCE) of the fabricated DSSCs was assessed by Enlitech QE-T spectral equipment.

## 3 Results and discussion

### 3.1 UV–Vis absorption spectra

The UV–Vis absorption spectra of dyes extracted in ethanol from *Arachis hypogaea* (AH), *Cassia grandis* (CG) and their combination (AC) in the absorption region between 300 and 700 nm are depicted in Fig. 3. In the spectra, *Arachis hypogaea* exhibits an absorption maximum at 425 to 485 nm corresponding to xanthophyll pigments from the family of carotenoids [21, 25]. In the same spectrum, there is also a trace of chlorophyll overlapped in the region between 410 and 440 nm that may be related to chlorophyll and would contribute to the absorption of solar energy. In the dye extract of *Cassia grandis* (CG), absorption peaks appear at 410 to 440 nm and 664 nm, associated to the presence of chlorophyll [26, 27]. Chlorophyll is an essential biomolecule involved in photosynthesis

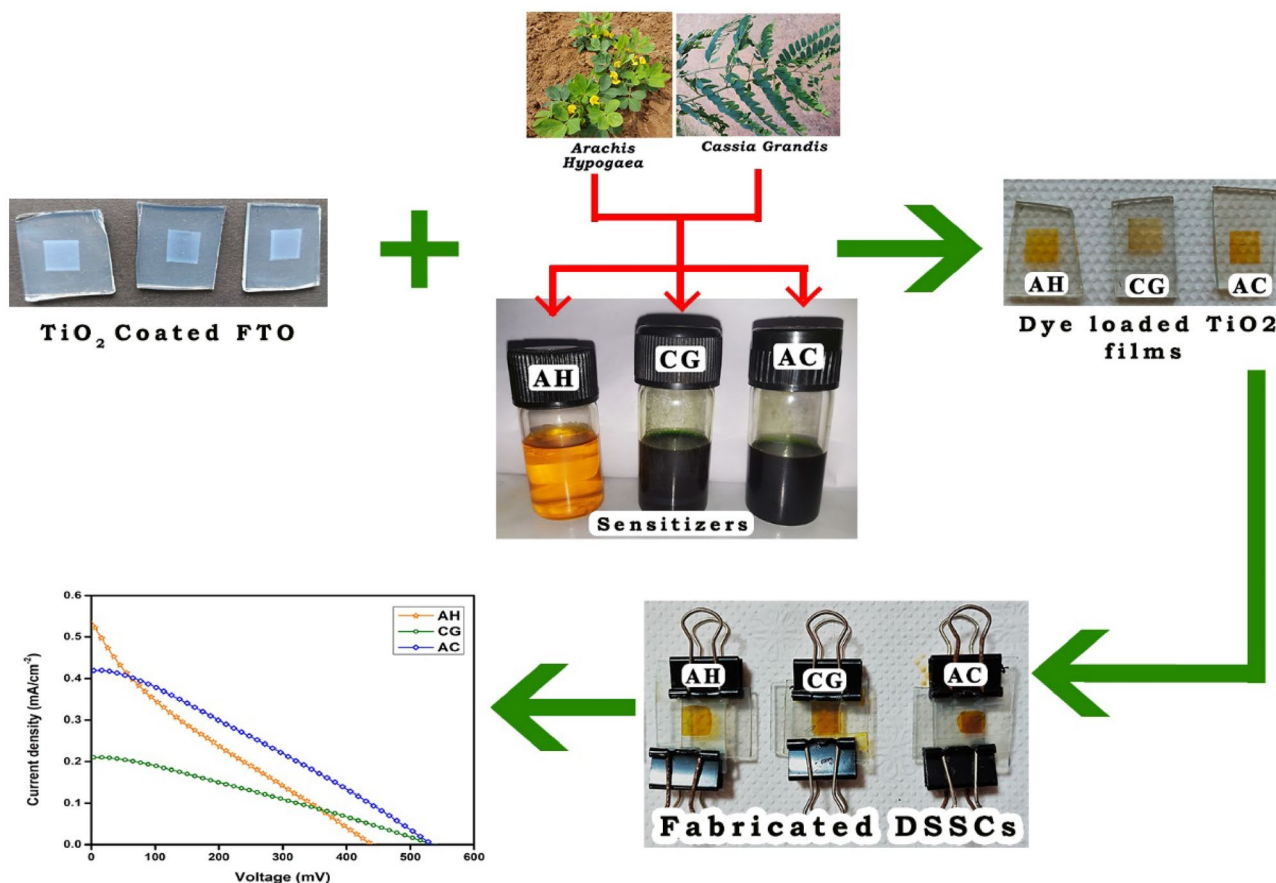


Fig. 2 Diagrammatic representation of AH, CG and AC device fabrication and performance

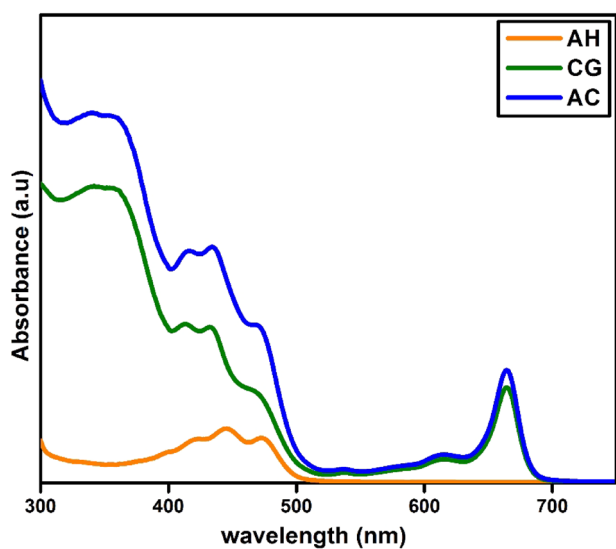


Fig. 3 UV-Vis absorption spectra of AH, CG and AC dyes in ethanol

that absorbs light in the blue and red regions of the visible spectrum [28].

In the spectrum of co-sensitized extract, AC shows enhanced light photon absorption with higher intensity than both AH and CG extracts. The wider peak at the blue region around 400–500 nm and 664 nm indicates the mixture of chlorophyll and xanthophyll pigments. This broadening can be ascribed to the ability of co-sensitized pigment to harvest a broader spectrum of solar energy which in turn could generate a higher photocurrent. The light harvesting efficiency of AC mixed dye is increased higher when AH and CG pigments are used in combination than when they are used independently. In the co-sensitized AC spectrum, there is no new additional absorption peak or peak shift except for the intensity variation. So it is obvious that the visible light absorption of the co-sensitized pigment AC in ethanol solution is the synergy of two single pigments AH and CG.

The absorption inception is taken into consideration to define the optical bandgap of the sensitizers

since it is the lowest energy at which an optical absorption occurs and resembles the shift between the upper and lower limits of the conduction and valence bands [12]. The optical energy bandgap of the sensitizers is derived using the following relationship:

$$\alpha h \frac{c}{\lambda} = A (h \frac{c}{\lambda} - E_g)^n \quad (1)$$

where  $\alpha$  denotes the absorption coefficient,  $h$  is the Planck constant,  $c$  is the speed of light,  $\lambda$  is the wavelength,  $E_g$  is the energy gap value,  $A$  is a parameter based on the optical probability and  $n$  designates the type of the optical transition. There are two different

types of transitions such as direct and indirect, of which one is permitted and the other is not. For the pure and co-sensitized dyes, the nature of the transition is a direct permitted optical transition with  $n = 1/2$  [29]. Therefore, Eq. (1) becomes:

$$(\alpha E)^2 = A (E - E_g) \text{ where } E = h \frac{c}{\lambda} \quad (2)$$

The direct bandgap ( $E_g$ ) of AH, CG and AC dye extracts (2.64 eV, 2.7 eV, 2.62 eV) is obtained from the intercept of a straight line on  $h\nu$  axis in a plot of  $(\alpha h\nu)^2$  versus  $h\nu$  as shown in Fig. 4.

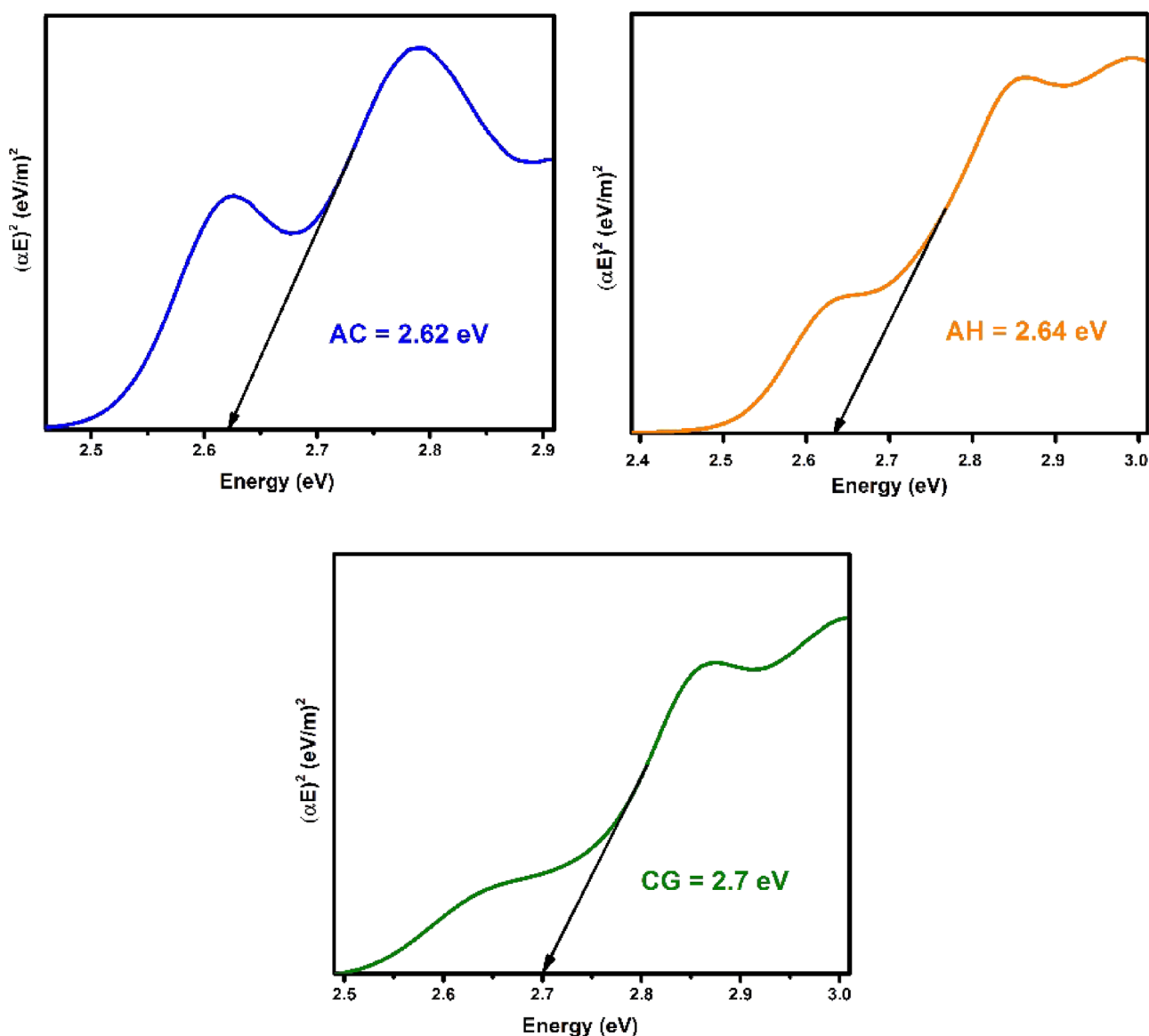


**Fig. 4** Bandgap of AH, CG and AC dye extracts using Tauc plot

### 3.2 Fourier transform Infra-red analysis

The functional groups in the FTIR spectra of the dyes AH, CG, and AC are identical as shown in Fig. 5. The peak at  $1056\text{ cm}^{-1}$  is attributed to C–O–C stretching vibrations of acid and carbohydrate groups while the peak at  $1085\text{ cm}^{-1}$  is related to C–O stretching vibration [30]. The vibrations of the C=N symmetric stretching and carbon–nitrogen carbon bending are caused by the strong peak emerging at  $1385\text{ cm}^{-1}$  [31]. The peak at  $1519\text{ cm}^{-1}$  is due to carbon–carbon double bonds of aromatic rings. The peaks at  $1263\text{ cm}^{-1}$  and  $1454\text{ cm}^{-1}$  are assigned to C–N stretching and C–H bending vibrations [32, 33].

The peak appearing at  $2974\text{ cm}^{-1}$  and  $2887\text{ cm}^{-1}$  correspond to aromatic CH stretching vibrations and to aliphatic CH groups. C=O stretching vibration shows a peak at  $1639\text{ cm}^{-1}$ . The broad peak from  $3000$  to  $3700\text{ cm}^{-1}$  is ascribed to –OH stretching due to the presence of alcohol groups [12, 34]. The presence of CO, OH functional groups in xanthophyll, chlorophyll and their mixtures (CG, AH, AC) makes them suitable as sensitizers in DSSCs, resulting in efficient binding with the photo electrode.

### 3.3 Field emission scanning electron microscopy (FESEM) and EDAX analysis

The surface morphology and microstructure of pure  $\text{TiO}_2$  and dye anchored  $\text{TiO}_2$  films are characterized

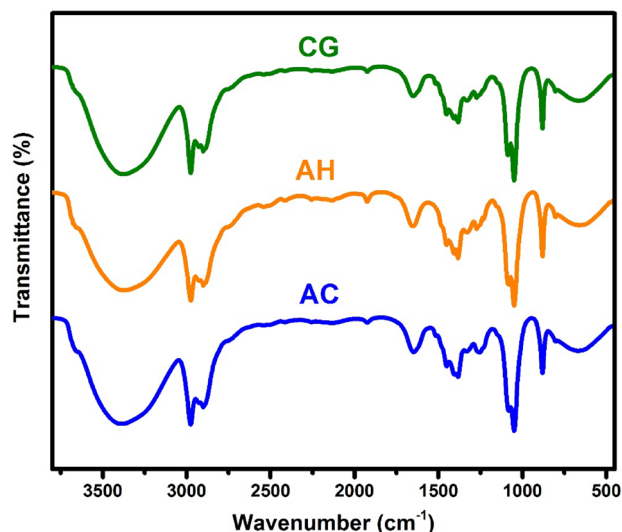


Fig. 5 FT-IR Spectra of AH, CG and AC dye extracts

by field emission scanning electron microscopy as shown in Fig. 6. The surface morphology of pure  $\text{TiO}_2$  has a significant impact on charge transit, dye adsorption, and collection of charges from the dye [35]. From Fig. 6(a), it is clear that the pure  $\text{TiO}_2$  film surface coatings are uniform, porous and made up entirely of spherical particles with no visible cracks. This ensures adequate dye adsorption and enhances efficient light harvesting. The adherence of xanthophyll, chlorophyll and combined dye pigments to the pure  $\text{TiO}_2$  films are supported by FESEM and depicted in Fig. 6.b, c and d. The surface of the  $\text{TiO}_2$  films has a significant difference both before and after dye staining. The surface of co-sensitized film AC is found with densely packed dye pigments compared to AH and CG films.

The elemental composition of pure  $\text{TiO}_2$  thin films are investigated by energy dispersive X-ray spectroscopy and illustrated in Fig. 7 with the chemical mapping of their respective elements. The presence of Ti and O elements are confirmed from the spectra. Ti contributes 55.5% of the total weight, O contributes 34.9%, C contributes 8.9%, and the remaining 0.7% is made up of various impurity elements.

### 3.4 Atomic force microscopy analysis

The surface morphology of  $\text{TiO}_2$  thin film is analyzed through atomic force microscopy. Figure 8 shows the 2D and 3D AFM analysis carried out, to study roughness, porosity and homogeneity of the anatase  $\text{TiO}_2$  films after annealing at  $450\text{ }^\circ\text{C}$ . The average roughness of  $\text{TiO}_2$  thin film is  $16.180\text{ nm}$  and the root mean square roughness is  $23.110\text{ nm}$  respectively. From the 2D image, the film is found to be uniformly coated and densely packed to absorb the dye molecules effectively. The 3D image shows the porous nature of titanium dioxide, coated on the FTO to be able to capture sensitizers on the surface which would further help in lower recombination and subsequently improve the conversion efficiency of the solar cell. Thus the obtained AFM results are in agreement with SEM results in terms of homogeneity, density and porosity.

### 3.5 Photovoltaic characteristics

The photovoltaic performance of AH, CG and AC sensitizers in the photo electrochemical solar cells are investigated through electrical current and voltage outputs under  $85\text{ mW/cm}^2$  illuminations as depicted in Fig. 9. The photo electrochemical characteristics of

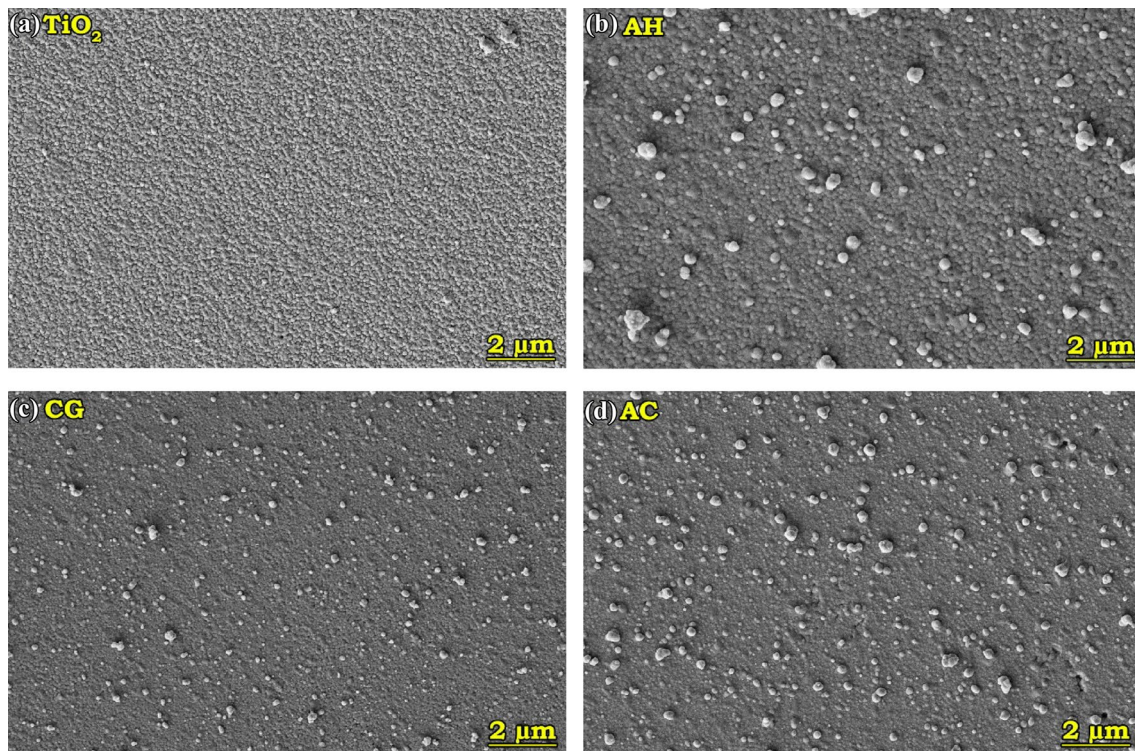


**Fig. 6** FESEM images of (a) pure  $\text{TiO}_2$  film (b) AH (c) CG and (d) AC dye loaded  $\text{TiO}_2$

the fabricated devices with AH, CG and AC sensitizers are determined by open-circuit voltage ( $V_{oc}$ ), short-circuit current density ( $J_{sc}$ ), maximum voltage ( $V_{max}$ ), maximum current ( $I_{max}$ ), fill factor (FF), and efficiency ( $\eta$ ) and tabulated in Table 2. On the basis of the photo current–voltage (I–V) curve, fill factor (FF) can be calculated as follows:

$$FF = \frac{J_{max} \times V_{max}}{J_{sc} \times V_{oc}} \quad (3)$$

where maximum power output ( $P_{max}$ ) is represented by maximum current density ( $J_{max}$ ) and maximum voltage ( $V_{max}$ ) respectively;  $V_{oc}$  is the open-circuit photo voltage and  $J_{sc}$  is the short-circuit current density. The overall solar conversion efficiency ( $\eta$ ) of the fabricated devices is defined by the formula:

$$\eta(\%) = \frac{J_{sc} \times V_{oc} \times FF}{P_{in}} \quad (4)$$

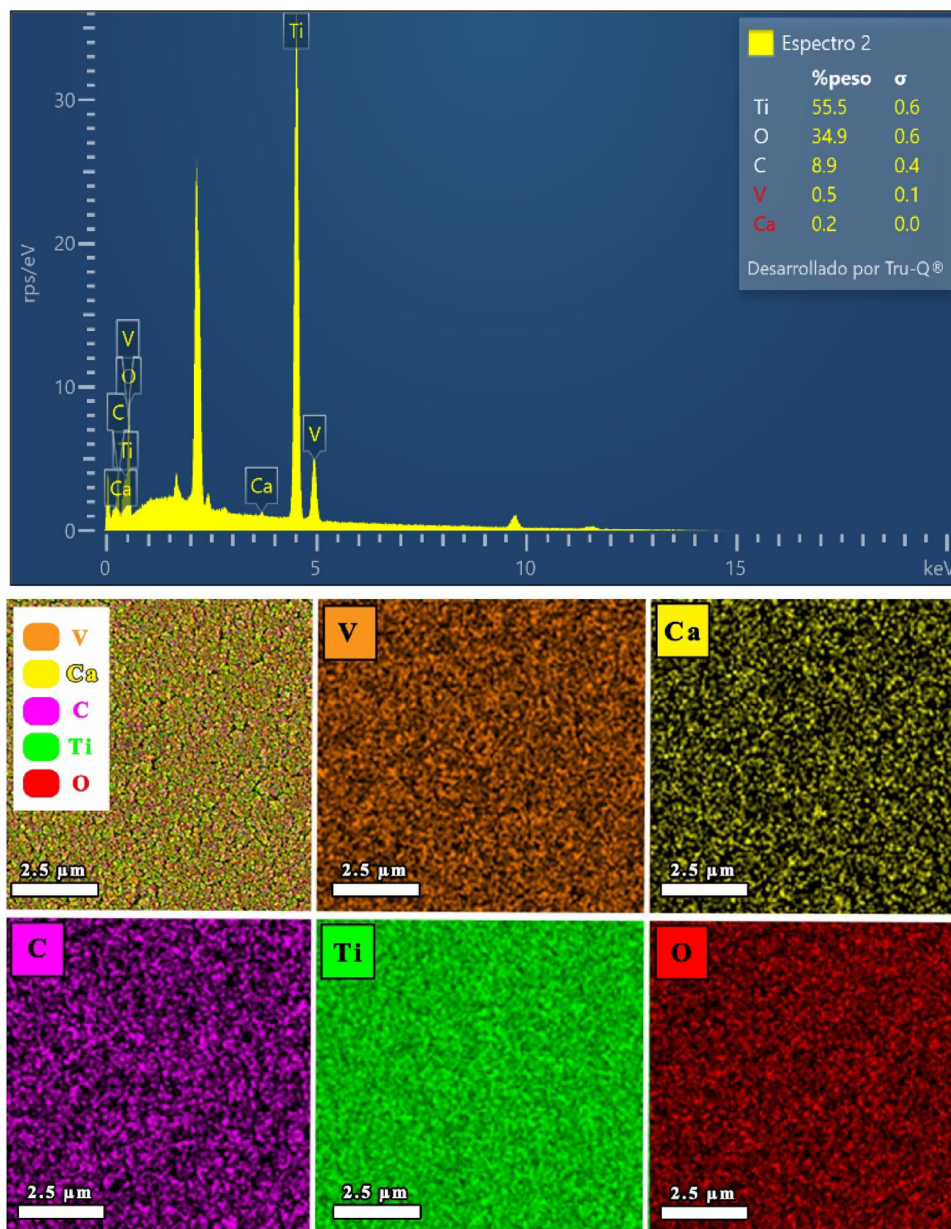
The chlorophyll dye based DSSC with *Cassia grandis* (CG) exhibits a cell efficiency of 0.36% with  $J_{sc}$  of  $0.208 \text{ mA cm}^{-2}$ ,  $V_{oc}$  of 532 mV and FF of 0.28. Xanthophyll often serves as the light-harvesting antenna

pigment in green plant photosystems, capturing and transmitting light energy to the pigment molecules in the reaction center rather than being photo electrochemically reactive. On the other hand, when xanthophyll is coupled with  $\text{TiO}_2$  electrode, it exhibits active photoelectrochemical activities [18] with the  $J_{sc}$  of  $0.537 \text{ mA cm}^{-2}$  and  $V_{oc}$  of 440 and FF of 0.195 which is higher than those of the chlorophyll based cells. Although there is not much of a difference between the open circuit voltages ( $V_{oc}$ ) of AH and CG, there is a significant difference between their current densities ( $J_{sc}$ ). The increase in the  $J_{sc}$  of AH cell could be related to efficient electron injection from the excited dyes into  $\text{TiO}_2$ .

The co-sensitized dye based DSSC AC, with combined dyes of AH and CG in 1:1 ratio displays the largest photovoltage and photocurrent and exhibits the cell efficiency of 0.76% with  $V_{oc}$  of 533 mV,  $J_{sc}$  of  $0.42 \text{ mA cm}^{-2}$  and FF of 0.29. This efficiency is 2.11 times higher than chlorophyll based cells and 1.4 times higher than xanthophyll based cells. When comparing all three fabricated devices (AH, CG, and AC), their photovoltaic performance follows a descending pattern of  $AC > AH > CG$ , (Fig. 10) where the co-sensitized dye-based cell AC exhibits an enhanced performance



**Fig. 7** EDAX measurement and elemental mapping of pure  $\text{TiO}_2$



compared to AH, followed by CG with individual dyes. This result is in good agreement with the absorption spectra, where AC was found to have a higher absorption than AH, followed by CG. The co-sensitized dye AC with higher absorption leads to higher efficiency in the fabricated devices as the device efficiency mainly depends on the absorption coefficient.

### 3.6 Electrochemical impedance spectroscopy analysis

Electrochemical impedance spectroscopy (EIS) is a potent method for comprehending the charge transport, ionic, interfacial kinetics and electronic processes in DSSC. In the present work the EIS spectra

**Fig. 8** 2D and 3D AFM images of TiO<sub>2</sub> thin films

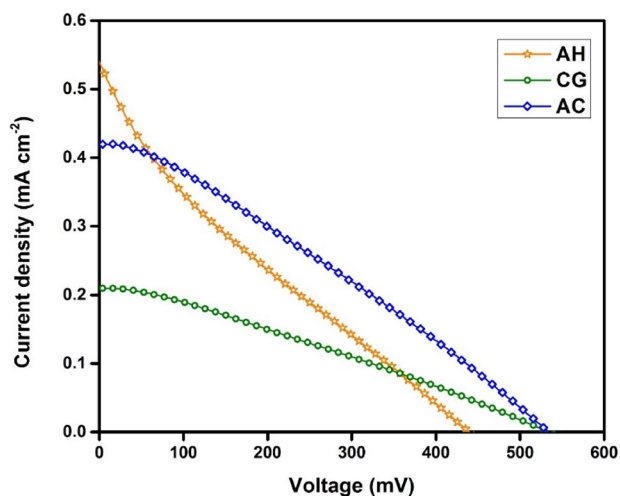
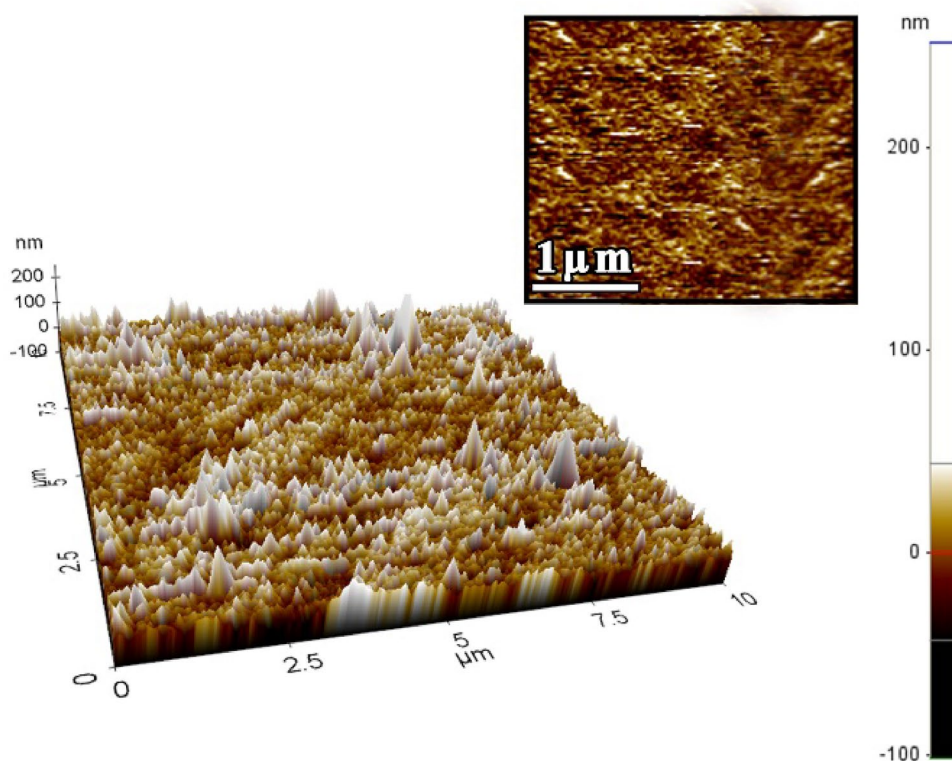


**Fig. 9** Current–Voltage curves of AH, CG and AC sensitized DSSCs

is recorded in the frequency range of 1 to 100 kHz and Nyquist plots of AH, CG and AC devices are presented in Fig. 11. The well-defined semi-circles observed in the high frequency region are explained by fitting the Nyquist data to the equivalent circuit model (Fig. 11 inset), which reveals the charge transfer resistance between the counter electrode and redox electrolyte. The charge-transfer resistance ( $R_{ct}$ ) within the cells could be obtained from the diameter of the semicircle. In the analysis of EIS spectra, it is found that the co-sensitized dye based DSSC AC shows less  $R_{ct}$  of 311.95  $\Omega$  compared to the AH and CG based solar cells with  $R_{ct}$  of 401.54  $\Omega$  and 824.94  $\Omega$  respectively as listed in Table 2. The results reveal that the increased  $R_{ct}$  in CG based DSSC is because of the poor electron generation leading to relatively high resistance to the flow of electron at TiO<sub>2</sub>/dye/electrolyte interphase [36]. This finding is supported by the lower light absorption of CG dye in the absorption spectra in

**Table 2** Solar cell parameters of AH, CG and AC devices

Dye	$J_{sc}$ (mA cm <sup>-2</sup> )	$V_{oc}$ (mV)	FF	$\eta$ %	$R_{ct}$ ( $\Omega$ cm <sup>-2</sup> )	$\tau$ (s) $\times 10^{-3}$
AH	0.537	440	0.195	0.54	401.54	2.30
CG	0.208	532	0.28	0.36	824.94	1.88
AC	0.42	533	0.29	0.76	311.95	4.94

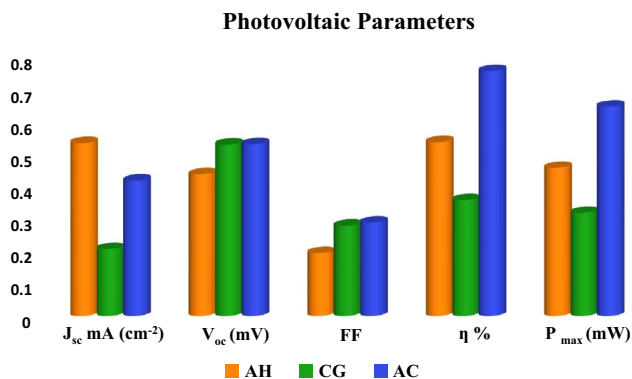


Fig. 10 Comparative diagram of the photovoltaic parameters in AH, CG and AC devices

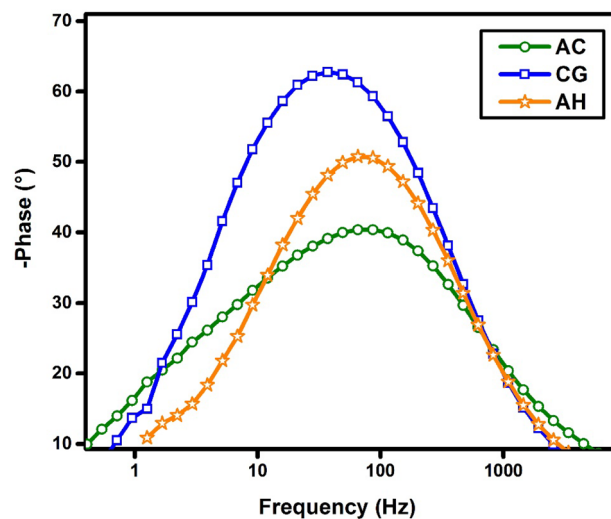


Fig. 12 Bode phase plots of AH, CG and AC devices

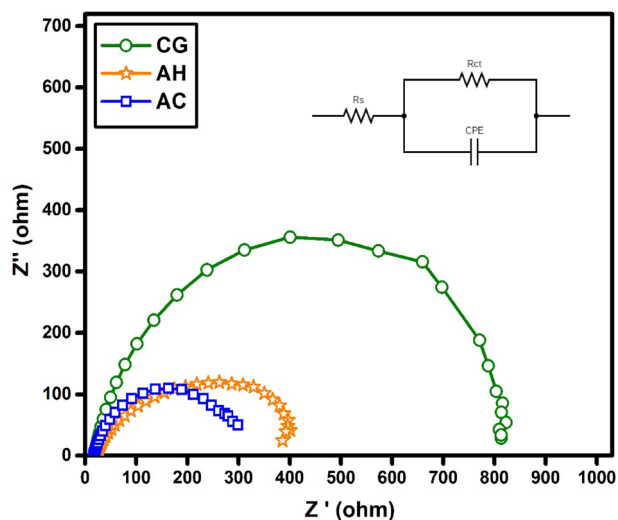


Fig. 11 Nyquist plots measured from EIS data for AH, CG and CG devices

Fig. 3. It is also observed from the absorption spectra that AC absorbs more energy than AH and CG, leading to electron-hole generation in the fabricated cell and therefore a low  $R_{ct}$ .

The Bode phase plots based on the impedance results are shown in Fig. 12. The electron life time in AH, CG and AC devices is calculated in Table.2 with the maximum angular frequency of the impedance semicircle in the mid frequency region, by using the formula.

$$\tau = \frac{1}{2\pi f_{max}} \tag{5}$$

where the highest mid-frequency peak is represented by  $f_{max}$ . Hence, a lower electron lifetime is indicated

by a frequency peak shifting to the higher frequency, and a higher electron lifetime is denoted by the shift to the lower frequency.

The obtained frequency ranges of AH, CG and AC are 69.11 Hz, 84.63 Hz and 32.22 Hz respectively. In the co-sensitized device AC, the peak frequency is shifted to the lower frequency region resulting in longer electron life time. When comparing the electron lifetimes of AH and CG, it is found that AH, which is based on xanthophyll, has a greater electron lifetime. The longer life time of the cell AC with co-sensitizers, indicates slower recombination, which is in good agreement with the J-V and impedance analysis.

### 3.7 Incident photon to current conversion efficiency (IPCE)

The incident photon-to-current conversion efficiency (IPCE) for AH, CG, and AC dye-based solar cells is measured in order to assess the effectiveness of natural dye in the performance of DSSCs. IPCE is calculated by dividing the monochromatic photon flux that strikes the cell by the number of electrons, as measured as photocurrent in the external circuit [23]. The IPCE values of DSSCs sensitized with AH, CG and AC are shown in Fig. 13. In the frequency region between 300 and 370 nm, the AC mixed extract shows a higher IPCE value of 18.8%, while the AH and CG individual extracts show values of 11.7 and 8.3%, respectively. Again, in the frequency range between 400 and 560 nm, AC mixed extract shows a higher

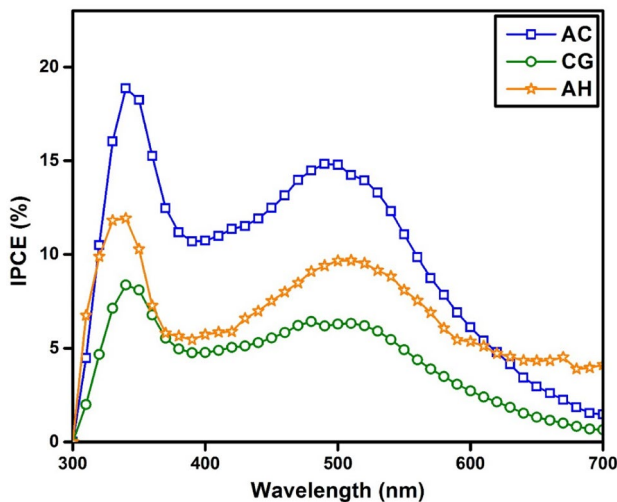


**Fig. 13** IPCE spectra of AH, CG and AC devices

IPCE value of 15.4%, and AH and CG individual dyes exhibit 9.6 and 6.5%, respectively. The higher IPCE value obtained with AC compared to AH and CG is also reflected in an overall increase in  $J_{sc}$ . The results obtained from IPCE spectra are in line with findings from UV–visible, I–V, and EIS analysis that indicated AC dye-based device to have a better conversion efficiency than AH and CG dye-based devices.

## 4 Conclusion

The fabrication of DSSCs using novel natural dyes from *A. hypogea*, *C. grandis* and their combination as sensitizers has been successfully done for the first time. The optical, structural, morphological, elemental analysis, current–voltage characteristics, impedance and electron life time analysis were performed to know the overall efficiencies of the fabricated devices AH, CG and AC. The obtained conversion efficiency for AH and GC was 0.54% and 0.36% respectively. The best prepared device with AC co-sensitizer showed highest efficiency of  $\eta = 0.76\%$  with  $V_{oc}$  of 533 mV,  $J_{sc}$  of  $0.42 \text{ mA cm}^{-2}$  and FF of 0.29. In the co-sensitized dye based DSSC (AC), the mixed dye performed synergistically, resulting in a high electron recombination resistant process that reduced electron recombination and increased overall cell performance. The photovoltaic performance of natural dye-based devices is typically lower than that of commercial dye-based devices, yet they exhibit greater economic and environmental

benefits. This continually draws the attention of the researchers to make modifications in the further research to build environmentally friendly solar cells.

## Author contributions

All authors contributed to the study conception and design. Material preparation, data collection and analysis were performed by AS and LRA. The first draft of the manuscript was written by AS and all authors commented on previous versions of the manuscript. All authors read and approved the final manuscript.

## Funding

The authors declare that no funds, grants, or other support were received during the preparation of this manuscript.

## Data availability

All data investigated through this study are included in this manuscript as figures and tables.

## Declarations

**Conflict of interest** The authors declare no conflict of interest.

## References

1. G. Richhariya, A. Kumar, P. Tekasakul, B. Gupta, *Renew. Sustain. Energy Rev.* **69**, 705 (2017)
2. N. Prabavathy, S. Shalini, R. Balasundaraprabhu, D. Velauthapillai, S. Prasanna, N. Muthukumarasamy, *Int. J. Energy Res.* **41**, 1372 (2017)
3. B. O'Regan, M. Grätzel, *Nature* **353**, 737 (1991)
4. H. Hug, M. Bader, P. Mair, T. Glatzel, *Appl. Energy* **115**, 216 (2014)
5. E.M. Abdou, H.S. Hafez, E. Bakir, M.S.A. Abdel-Mottaleb, *Spectrochim. Acta Part A Mol. Biomol. Spectrosc.* **115**, 20 (2013)
6. A. Arulraj, S. Govindan, S. Vadivel, B. Subramanian, *J. Mater. Sci. Mater. Electron.* **28**, 18455 (2017)

7. P.A. Ahmad, F.A. Mir, F. Ullah, M.A. Bhat, M.H. Rather, *Opt. Quantum Electron* **55**, 1 (2023)
8. A. Omar, M.S. Ali, N. Abd Rahim, *Sol. Energy* **207**, 1088 (2020)
9. G.F.C. Mejica, Y. Unpaprom, D. Balakrishnan, N. Dusadee, S. Buochareon, R. Ramaraj, *Sustain. Energy Technol. Assess.* **51**, 101971 (2022)
10. K.A. Kumar, K. Subalakshmi, J. Senthilselvan, *A.I.P. Conf. Proc.* **1731**, 1 (2016)
11. D. Ganta, J. Jara, R. Villanueva, *Chem. Phys. Lett.* **679**, 97 (2017)
12. N. Patni, S.G. Pillai, P. Sharma, *Int. J. Energy Res.* **44**, 10846 (2020)
13. M. Golshan, S. Osfouri, R. Azin, T. Jalali, N.R. Moheimani, *J. Photochem. Photobiol. A Chem.* **417**, 113345 (2021)
14. S. Shah, M.H. Buraidah, L.P. Teo, M.A. Careem, A.K. Arof, *Opt. Quantum Electron.* **48**, 1 (2016)
15. S.C. Ezike, C.N. Hyelnasinyi, M.A. Salawu, J.F. Wansah, A.N. Ossai, N.N. Agu, *Surf. Interf.* **22**, 100882 (2021)
16. F. Kabir, M.M.H. Bhuiyan, M.S. Manir, M.S. Rahaman, M.A. Khan, T. Ikegami, *Results Phys.* **14**, 102474 (2019)
17. N.T.R.N. Kumara, P. Ekanayake, A. Lim, L.Y.C. Liew, M. Iskandar, L.C. Ming, G.K.R. Senadeera, *J. Alloys Compd.* **581**, 186 (2013)
18. B.-Q. Liu, X.-P. Zhao, W. Luo, *Dye. Pigment.* **76**, 327 (2008)
19. A. Arulraj, G. Senguttuvan, S. Veeramani, V. Sivakumar, B. Subramanian, *Optik (Stuttg.)* **181**, 619 (2019)
20. A. Soosairaj, A. Gunasekaran, S. Anandan, and L. R. Asirvatham, (2023) *Environ. Sci. Pollut. Res.*
21. A. Lim, N. Haji Manaf, K. Tennakoon, R.L.N. Chandrakanthi, L.B.L. Lim, J.M.R.S. Bandara, P. Ekanayake, *J. Biophys.* (2015). <https://doi.org/10.1155/2015/510467>
22. H.A. Maddah, V. Berry, S.K. Behura, *Renew. Sustain. Energy Rev.* **121**, 109678 (2020)
23. R. Ramamoorthy, N. Radha, G. Maheswari, S. Anandan, S. Manoharan, R. Victor Williams, *J. Appl. Electrochem.* **46**, 929 (2016)
24. A. Gunasekaran, A. Sorrentino, A.M. Asiri, S. Anandan, *Sol. Energy* **208**, 160 (2020)
25. D. Dodoo-Arhin, R.C.T. Howe, G. Hu, Y. Zhang, P. Hiralal, A. Bello, G. Amaratunga, T. Hasan, *Carbon N. Y.* **105**, 33 (2016)
26. C. Cari, K. Khairuddin, T. Y. Septiawan, P. M. Suciatioko, D. Kurniawan, and A. Supriyanto, (2018) *AIP Conf. Proc.*
27. P. Khammee, Y. Unpaprom, K. Whangchai, R. Ramaraj, *Biomass Convers. Biorefinery* **12**, 1619 (2022)
28. G. Calogero, I. Citro, C. Crupi, G. Carini, D. Arigò, G. Spinella, A. Bartolotta, G. Di Marco, *Opt. Mater. (Amst.)* **88**, 24 (2019)
29. R. Anoua, H. Lifi, S. Touhtouh, M. El Jouad, A. Hajjaji, M. Bakasse, P. Płociennik, A. Zawadzka, *Environ. Sci. Pollut. Res. Int.* **28**, 57860 (2021)
30. A.M. Ammar, H.S.H. Mohamed, M.M.K. Yousef, G.M. Abdel-Hafez, A.S. Hassaniien, A.S.G. Khalil, J. Nanomater. (2019). <https://doi.org/10.1155/2019/1867271>
31. K.V. Hemalatha, S.N. Karthick, C. Justin Raj, N.Y. Hong, S.K. Kim, H.J. Kim, *Spectrochim. Acta - Part A Mol. Biomol. Spectrosc.* **96**, 305 (2012)
32. T. Montagni, P. Enciso, J.J. Marizcurrena, S. Castro-Sowinski, C. Fontana, D. Davyt, M.F. Cerdá, *Environ. Sustain.* **1**, 89 (2018)
33. S. Mathew, N. Sajina, K.R. Haridas, *Chemist* **89**, 2 (2016)
34. K. Mensah-Darkwa, F.O. Agyemang, D. Yeboah, S. Akromah, *Mater. Today Proc.* **38**, 514 (2021)
35. G. Genifer Silvena, B. JohnR. Anne Sarah Christinal MC. Santhosh Kumar S. Chakravarty A. Leo Rajesh, *J Inorg Organomet Polym Mater* **27**, 1556 (2017)
36. T. Raguram, K.S. Rajni, *J. Sol-Gel Sci. Technol.* **93**, 202 (2020)

**Publisher's Note** Springer Nature remains neutral with regard to jurisdictional claims in published maps and institutional affiliations.

Springer Nature or its licensor (e.g. a society or other partner) holds exclusive rights to this article under a publishing agreement with the author(s) or other rightsholder(s); author self-archiving of the accepted manuscript version of this article is solely governed by the terms of such publishing agreement and applicable law.